Journal of Alloys and Compounds 506 (2010) 313–316

Contents lists available at ScienceDirect

Journal of Alloys and Compounds

journal homepage: www.elsevier.com/locate/jallcom

The phase evolution with temperature in $0.94PbZrO_3$–$0.06Pb(Mg_{1/2}W_{1/2})O_3$ antiferroelectric ceramic

Piyanut Charoonsuk[a,b], Supamas Wirunchit[a,b], Rangson Muanghlua[c], Surasak Niemcharoen[c], Banjong Boonchom[d], Naratip Vittayakorn[a,b,e,*]

[a] Electroceramic Research Laboratory, College of KMITL Nanotechnology, King Mongkut's Institute of Technology Ladkrabang, Bangkok 10520, Thailand
[b] ThEP Center, CHE, 328 Si Ayutthaya Rd., Bangkok 10400, Thailand
[c] Department of Electronics, Faculty of Engineering, King Mongkut's Institute of Technology Ladkrabang, Bangkok 10520, Thailand
[d] King Mongkut's Institute of Technology Ladkrabang, Chumphon Campus, 17/1M. 6 Pha Thiew District, Chumphon 86160, Thailand
[e] Advanced Materials Science Research Unit, Department of Chemistry, Faculty of Science, King Mongkut's Institute of Technology Ladkrabang, Bangkok 10520, Thailand

ARTICLE INFO

Article history:
Received 14 May 2010
Received in revised form 28 June 2010
Accepted 30 June 2010
Available online 7 July 2010

Keywords:
Antiferroelectric
Wolframite precursor method
Lead Zirconate
Lead Magnesium Tungstate

ABSTRACT

The perovskite structure of the lead zirconate–lead magnesium tungstate ceramic, $0.94PbZrO_3$–$0.06Pb(Mg_{1/2}W_{1/2})O_3$ (0.94PZ–0.06PMW), was prepared by the wolframite precursor method. The phase evolution with temperature in the 0.94PZ–0.06PMW ceramic was investigated, with dielectric permittivity, differential scanning calorimetry and polarization measurements. The ceramic was in the antiferroelectric phase when below 177 °C, based on dielectric measurement, and an intermediate phase was detected between 177 and 219 °C. Evidence from ferroelectric data was found to suggest that this intermediate phase is ferroelectric.

1. Introduction

Active studies of antiferroelectric (AFE) materials have been recently enhanced for next-generation electronic systems, for example, microelectromechanical systems consisting of sensors and actuators and high performance energy storage devices [1,2]. The phase transition from AFE to the field-forced ferroelectric (FE) state, induced by an electric field [3,4], is characterized by typical double P–E hysteresis loops. These materials are suitable for nonlinear charge storage capacitors because a field-forced ferroelectric state releases all polarized charges and can therefore supply very high instantaneous currents at the ferroelectric to antiferroelectric reverse phase transition. Recently, AFE materials, including $Pb(Zr,Ti)O_3$, $(Pb,Ba)ZrO_3$, $(Pb,Sr)TiO_3$, $(Pb,La)(Zr,Ti)O_3$, $NaNbO_3$, and $(Bi_{0.5}Na_{0.5})TiO_3$ systems, have attracted increasing scientific attention [3–9]. Among them, lead zirconate ($PbZrO_3$; PZ) and $PbZrO_3$-based are the most attractive AFE materials, due to their high longitudinal strain response, and the latter is a proto-type of AFE ceramics that belongs to an ABO_3-type perovskite family of oxides [10,11]. At temperatures below the Curie temperature (230 °C), PZ displays an orthorhombic perovskite structure with lattice parameters of $a = 5.87$ Å, $b = 11.74$ Å and $c = 8.20$ Å [12]. This structure possesses an antiparallel shift of Pb ions along the [1 1 0], resulting in antiferroelectricity [13]. At temperatures above 230 °C, $PbZrO_3$ is in the paraelectric phase, with cubic $m3m$ symmetry [13,14]. An intermediate phase, characterized by $1/2\{1\,1\,0\}_c$-type superlattice diffractions, is in between the AFE and paraelectric phase, within a narrow temperature range of 225–230 °C [13,14]. It is well known that the AFE to FE phase transformation in PZ ceramic requires a very strong electric field; otherwise, dielectric breakdown occurs. Consequently, most commercial AFE ceramics are chemically modified by adding Ba^{2+}, Sr^{2+}, Ti^{4+} or Sn^{4+} to reduce the critical field and optimize the physical and electrical properties [3–9]. Sawaguchi [15] studied the effect of Ti^{4+} substitution in PZ on temperature variation of the P–E hysteresis loop and established the ferroelectric intermediate phase between the AFE and PE phase. Shirane [16] investigated the phase transition behavior of Ba^{2+} doping in PZ and reported that the ferroelectric intermediate phase between the AFE and PE phase for Ba^{2+} concentrations was lower than $x = 0.175$. Pokharel and Pandey [17,18] reported that relaxor ferroelectric behavior for Ba^{2+} concentrations was higher than $x = 0.25$. Recently, it was reported that antiferroelectric $(Pb_{1-x}Ba_x)ZrO_3$ (PBZ) films, with a higher barium content of more than 45 mol%, were in paraelectric state at room temperature and possessed excellent dielectric properties comparable to $(Ba,Sr)TiO_3$ [6]. On the contrary, a ferroelectric intermediate phase was not observed in lanthanum doping in PZ. Otherwise, lanthanum

* Corresponding author at: Department of Chemistry, Faculty of Science, King Mongkut's Institute of Technology Ladkrabang, Bangkok 10520, Thailand.
E-mail address: naratipcmu@yahoo.com (N. Vittayakorn).

0925-8388/$ – see front matter © 2010 Elsevier B.V. All rights reserved.
doi:10.1016/j.jallcom.2010.06.197

doping in PZ would be found to increase the stability range of the antiferroelectric phase [19,20]. Furthermore, Tan et al. [20] studied the doping effect of various metal oxide elements on field-induced polarization in PZ ceramics and found that addition of Bi^{3+} and K^{+} substantially increased stability of the antiferroelectric phase. Chen et al. [21] observed antiferroelectric-like or double hysteresis loops behavior in (Pb,Sr)TiO_3. However, the antiferroelectric nature is different from PZ ceramics. Rubia et al. [22] investigated the effect of Hf^{4+} substitution in PZ on phase transition, when the intermediate phase was found to increase with increasing Hf^{4+} concentrations. Up to now, scientific information about the effect of metal oxide substitution in PZ and nature of the intermediate phase is still unclear. Recently, our research work reported that the intermediate phase can also be introduced by partial replacement of Zr^{4+} ions with complex B-site ions such as Ni^{2+}/Nb^{5+} [23,24], Zn^{2+}/Nb^{5+} [25], or Co^{2+}/Nb^{5+} [26]. Furthermore, our previous study found that by adding minor amounts (2–10 mol%) of antiferroelectric $Pb(Mg_{1/2}W_{1/2})O_3$ (PMW) into antiferroelectric PZ, the temperature range expanded to an intermediate phase, which was characterized by evident frequency dispersion in dielectric permittivity [27]. As a consequence, a series of outstanding phase transitions were revealed by the dielectric measurement [27]. Nevertheless, the nature of the intermediate phase is still open for debate. The $0.94PbZrO_3$–$0.06Pb(Mg_{1/2}W_{1/2})O_3$ ceramic was selected in this study for further investigation of phase transformation sequence, while heating to 250 °C with ferroelectric measurement.

2. Experimental procedures

The perovskite structure of the lead zirconate–lead magnesium tungstate ceramic, $0.94PbZrO_3$–$0.06Pb(Mg_{1/2}W_{1/2})O_3$ (0.94PZ–0.06PMW), was prepared by the wolframite precursor method via the ball-milling technique. The wolframite structure ($MgWO_4$) was synthesized first before stoichiometric amounts of the precursor (MgO and WO_3) were mixed and milled in ethyl alcohol for 18 h. The mixture was then dried and calcined at 1100 °C for 4 h, and $MgWO_4$ and ZrO_2 were subsequently mixed with PbO. After re-milling and drying, the mixtures were calcined at 900 °C for 4 h in a closed alumina crucible. Pellets measuring 15 mm in diameter were pressed using 5% PVA, the binder was burned out slowly by heating to 500 °C over 2 h, and the samples were sintered at 1150 °C for 4 h. Phase formation of 0.94PZ–0.06PMW was investigated by X-ray diffraction (XRD). Scanning electron microscopy (SEM; Hitachi, s4007) was employed to investigate the microstructure of the sintered pellets. The major faces of the samples were lapped to determine their dielectric and ferroelectric properties, and silver electrodes were made from a low-temperature silver paste by firing at 550 °C for 30 min to enable electrical measurements to be taken. The relative permittivity (ε_r) and dissipation factor ($\tan\delta$) were measured using an HP-4284A LCR meter. The capacitance and dissipation factors of the sample were measured at 1–100 kHz, and the temperature varied between 25 and 350 °C. A heating rate of 2 °C/min was used during measurement, and the phase transitions also were measured by differential scanning calorimeter (DSC 2920, TA Instrument) between ambient temperature and 350 °C at a rate of 10 °C/min. The electrical polarization versus field hysteresis loops was recorded at a series of temperatures by a standardized ferroelectric test system (RT-66A, Radiant Technologies). The peak field was maintained at 30 kV/cm during measurement, and the ferroelectric hysteresis loop was recorded after the temperature was stabilized for at least 5 min.

3. Results and discussion

The XRD pattern of 0.94PZ–0.06PMW ceramic is presented in Fig. 1. The 0.94PZ–0.06PMW ceramic was identified from the patterns as a single-phase material with a perovskite structure having orthorhombic symmetry. Evidence of the pyrochlore or other second phases was not detected in the pattern, but the 1/4($h\,k\,l$) superstructure lines were present in the 0.94PZ–0.06PMW ceramic, indicating that the Pb^{2+} ions suffer antiparallel displacements with respect to their original position in the cubic perovskite lattice. The indexed pattern with the least number of refinement squares gave a cell with dimensions of $a = 5.85(1)$ Å, $b = 11.67(3)$ Å and $c = 8.16(8)$ Å. The cell parameters of 0.94PZ–0.06PMW were close to those of the standard data: PDF#751607 [$a = 5.88(4)$, $b = 11.76(0)$ and $c = 8.22(0)$]. A 97.8% relative density of the ceramic was measured

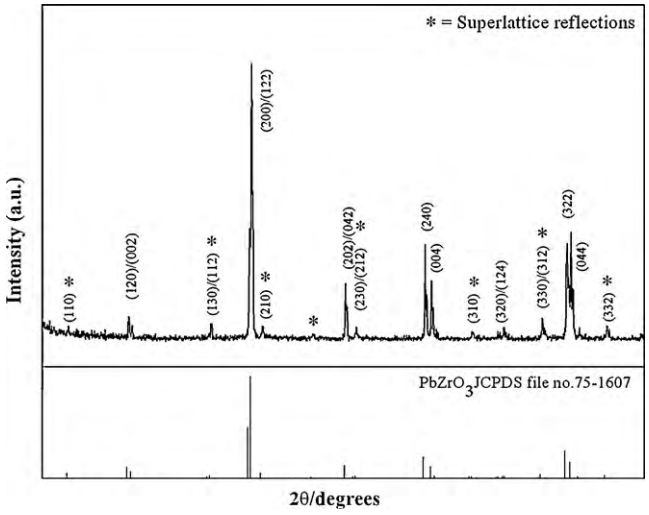

Fig. 1. XRD pattern of 0.94PZ–0.06PMW ceramic.

using the Archimedes method, and the grain size was examined by scanning electron microscopy (SEM). The fresh surface of the 0.94PZ–0.06PMW ceramic was almost free of pores, with a grain size in the range of 10–14 μm, as shown in Fig. 2.

The temperature dependence of relative permittivity and dielectric loss was measured at frequencies of 1, 10 and 100 kHz, while heating from 25 to 350 °C, and the results are displayed in Fig. 3. There were clearly two abrupt changes in both relative permittivity and dielectric loss in the 0.94PZ–0.06PMW ceramic. The first one occurred at around 177 °C, where both relative permittivity and dielectric loss increased by one order of magnitude. The other one took place at the Curie temperature of 219 °C, where significant suppression of dielectric loss was seen. Therefore, the dielectric response in the 0.94PZ–0.06PMW ceramic can be divided into three stages. At temperatures below 177 °C, both the relative permittivity and the dielectric loss have low values and show negligible increases with increasing temperatures. At temperatures above 219 °C, the relative permittivity begins to decrease following the Curie–Weiss law [3,4]. In the intermediate temperature range (177–219 °C), the relative permittivity increases dramatically, while the dielectric loss remains high at around 0.08.

To elucidate further on the dielectric behavior of different phases in the 0.94PZ–0.06PMW ceramic, electrically polarized hysteresis loop measurements were performed at a series of tem-

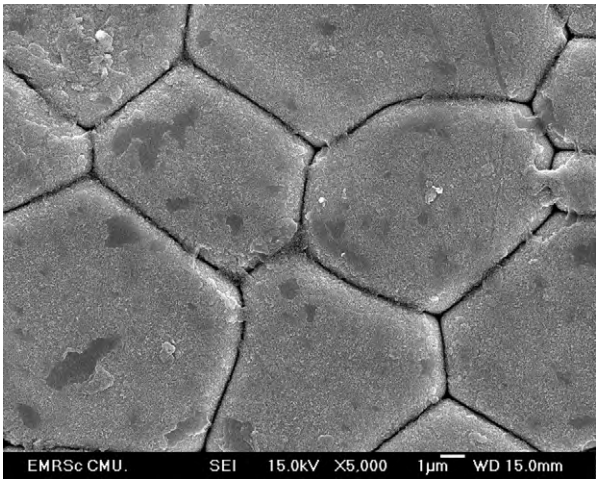

Fig. 2. SEM image of 0.94PZ–0.06PMW ceramic surfaces.

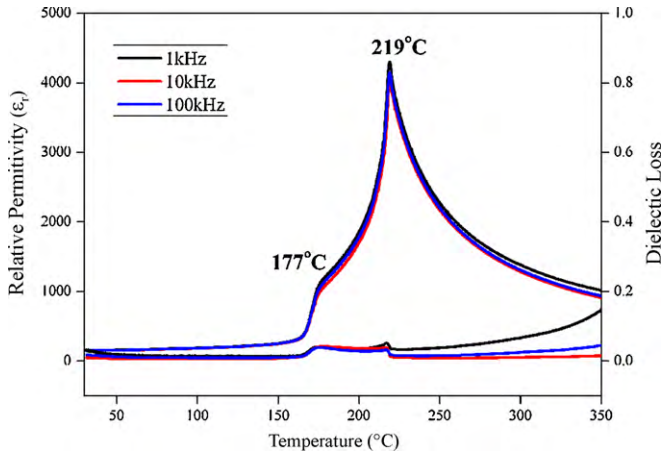

Fig. 3. Dielectric properties during heating at 1, 10 and 100 kHz in a bulk 0.94PZ–0.06PMW ceramic.

peratures under a peak field of 30 kV/cm. A circular disk specimen, with a diameter of about 10 mm and thickness of around 800 μm, was used. The loop was recorded after the temperature had been stabilized for at least 5 min. Linear polarization was displayed as a function of electric field between room temperature and 155 °C, as shown in Fig. 4(a)–(d). This could indicate that the 0.94PZ–0.06PMW ceramic has AFE behavior between room temperature and less than 150 °C [Fig. 4(a)]. Regarding bulk AFE ceramic specimens, the net remnant polarization (P_r) was zero, due to the existence of antiparallel dipole moments. To induce an AFE–FE phase transition, an intense electric field needs to be applied to the ceramics.

Hysteretic behavior starts to develop when the temperature increases to 155 °C, and a regular hysteresis loop has a coercive E_C field of 8.29 kV/cm, as shown in Fig. 4(b). However, the hysteresis loop observed does not indicate the presence of a ferroelectric phase. As seen in Fig. 4(b), close examination of the hysteresis loop at 155 °C reveals that slight distortions, which are marked by two circles, occurred at ~10 kV/cm. Similar distortions were found on the hysteresis loop in $0.98PbZrO_3$–$0.02Pb(Ni_{1/3}Nb_{2/3})O_3$ and $Pb_{0.99}Nb_{0.02}[Zr_{0.57}Sn_{0.43}]_{1-x}Ti_x]_{0.98}O_3$ ceramics, and these have been attributed to the onset of electric field-induced AFE to FE transition [28,29]. Therefore, the 0.94PZ–0.06PMW ceramic is still in the AFE phase at this temperature and it should be noted that the distortions marked at 155 °C in Fig. 4(b) indicate the AFE–FE phase transition. A regular hysteresis loop, exhibiting ferroelectricity, clearly demonstrated the intermediate phase between the AFE and PE phase when the temperature was raised to 190 °C [Fig. 4(c)]. Moreover, hysteretic behavior transition from the FE to PE phase occurred when the temperature increased to over 220 °C [Fig. 4(d)]. It is well known that the occurrence of antiferroelectricity in pure PZ is due to an antiparallel shift of Pb ions along the [1 1 0] direction and it also results in a superstructure line in the XRD pattern. It is apparent that replacement of the Zr^{4+} ion by Mg^{2+}/W^{6+} ions decreases the driving force for the antiparallel shift of Pb^{2+} ions, because they interrupt the translational symmetry. This interruption causes the appearance of an intermediate ferroelectric phase and similar behavior has been found in PZ–PNN ceramics [28].The DSC technique was used as the third tool to confirm the phase transition of PZ–PMW ceramics. Fig. 5 shows the temperature dependence of the heat flow (DSC curves) obtained when heating the 0.94PZ–0.06PMW sample at a rate of 10 °C/min. Two phase transitions in the 0.94PZ–0.06PMW ceramic were obtained with dielectric measurement and clearly confirmed by DSC measurement. The lower temperature of 163 °C corresponded to the transition temperature of the AFE → FE phase transition, while the higher one (215 °C) corresponded to the FE → PE phase transition. It is interesting to note that the difference in values of AFE–FE and FE–PE transition temperature in dielectric, ferroelectric and DSC measurement techniques is due to that in heating

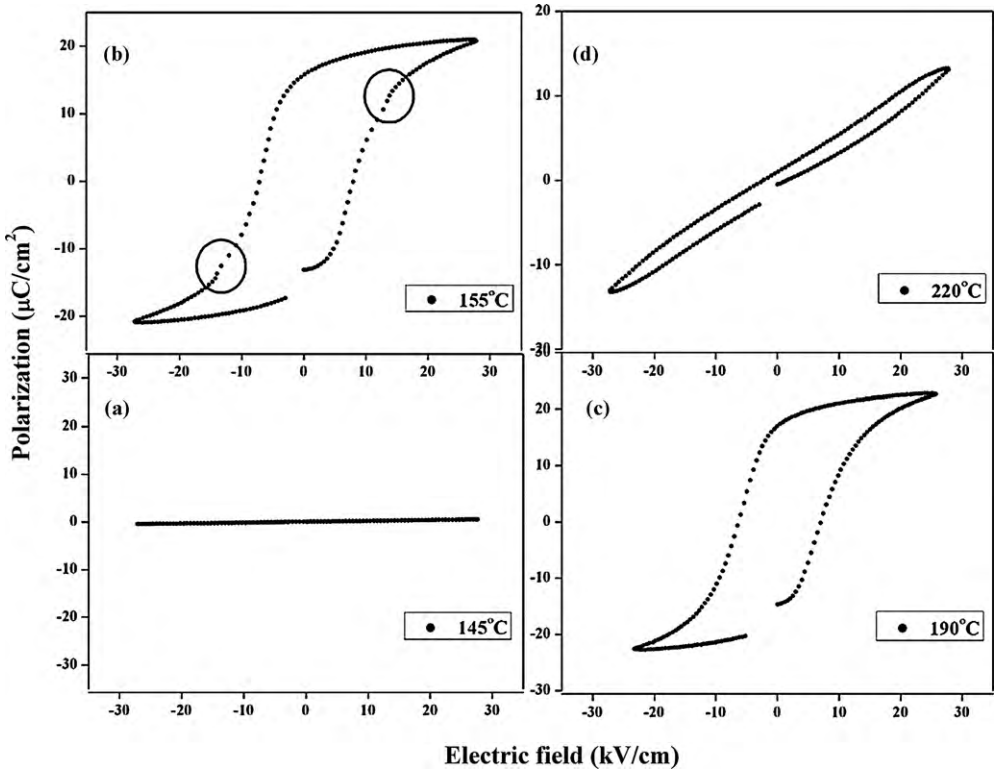

Fig. 4. Hysteresis loops of 0.94PZ–0.06PMW ceramic from temperatures of 145–220 °C.

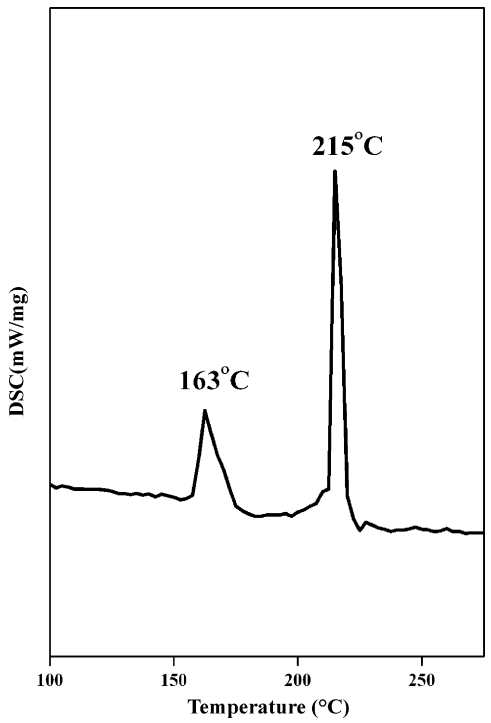

Fig. 5. DSC curves of 0.94PZ–0.06PMW ceramic.

rate and dwell time measurement. Thermodynamic parameter, enthalpy (ΔH^*/J g^{-1}), heat capacity (C_p/J g^{-1} K^{-1}), entropy change (ΔS^*/J g^{-1} K^{-1}), and Gibbs energy change (ΔG^*/J g^{-1}) were calculated from the DSC results. The enthalpy change was calculated directly from the amount of heat change involved in each step per unit mass of the sample. The ΔH^* was thus determined and implemented to calculate the specific heat capacity (C_p) using the following equation [30,31]:

$$C_p = 2.303 C_p \log(T_2/T_1) \quad (1)$$

where $\Delta T = T_2 - T_1$, T_1 is the temperature at which the DSC peak begins to depart from the baseline, and T_2 is the temperature at which the peak lands. Consequently, the changes of entropy (ΔS^*) and Gibbs energy (ΔG^*) were calculated using the following equations [30,31]:

$$\Delta S* = 2.303 C_p \log(T_2/T_1) \quad (2)$$

$$\Delta H* = \Delta G* - T_p \Delta S* \quad (3)$$

On the basis of DSC data, the value of ΔH^*, ΔS^*, C_p and ΔG^* for the phase transition can be calculated according to Eqs. (1)–(3), which are presented in Table 1. In terms of the activated complex theory (transition theory), the higher value of ΔS^* for the AFE to FE phase transition indicates a lower ordered activated complex. Also, the degree of rotation freedom as well as vibration is higher than that in non-activated complex antiferroelectric and paraelectric phases, which corresponds well with the formation of a non-stability phase. This means that the rate of AFE to FE phase transition is higher than that of the FE to PE phase transition of thermal transformation. Therefore, the FE to PE transformation step occurs harder than the AFE to FE transformation step. On the other hand, the thermodynamic parameter, $\Delta H^*$and ΔG^*, was calculated according to Eqs. (1)–(3) and gave the positive values for both steps, thus indicating that the AFE to FE to PE phase transitions are connected to the introduction of heat, and phase transitions are non-spontaneous processes.

Table 1
Values of thermodynamic parameters for phase transition of 0.94PZ–0.06PMW ceramics calculated from DSC data.

Temperature ranges/K	T_p/K	ΔH^*/J g^{-1}	C_p/J g^{-1} K^{-1}	ΔS^*/J g^{-1} K^{-1}	ΔG^*/J g^{-1}
431–441	436	1.207	2.768×10^{-3}	6.350×10^{-5}	1.179
487–491	488	2.325	4.764×10^{-3}	3.858×10^{-5}	2.308

4. Conclusions

The investigation of 0.94PZ–0.06PMW ceramics using XRD, dielectric behavior, differential scanning calorimetry and ferroelectric measurements has clearly shown a series of phase transitions that occur above room temperature. When the ceramic is in an antiferroelectric nature below 177 °C, both the dielectric property and the loss tangent are low and stable against temperature change. One order of magnitude increase in dielectric property occurs at around 177 °C, and loss tangent results within a narrow temperature range. The ceramic is in an intermediate phase at a temperature range of 177–219 °C, when it is believed to be ferroelectric. When the ceramic is above 219 °C, it is in the cubic paraelectric phase, with relative permittivity following the Curie–Weiss law. A thermodynamic parameter indicated that the AFE to FE to PE phase transitions are connected to the introduction of heat, and phase transitions are non-spontaneous processes.

Acknowledgements

This research was supported by a grant from the Thailand Research Fund (TRF), the Royal Golden Jubilee Ph.D. Program, and the National Nanotechnology Center (NANOTEC) NSTDA, Ministry of Science and Technology, Thailand, through its “Center of Excellence Network” program.

References

[1] G.R. Love, J. Am. Ceram. Soc. 73 (2005) 323–328.
[2] G.H. Haertling, J. Am. Ceram. Soc. 82 (1999) 797–818.
[3] Y. Xu, Ferroelectric Materials and Their Application, Elsevier Science Publishers B.V., Amsterdam, 1991.
[4] B. Jaffe, W.R. Cook, H. Jaffe, Piezoelectric Ceramics, Academic Press, London, 1971.
[5] L.B. Kong, J. Ma, W. Zhu, O.K. Tan, J. Alloys Compd. 322 (2001) 290–297.
[6] X. Hao, Z. Zhang, J. Zhou, S. An, J. Zhai, J. Alloys Compd. 501 (2010) 358–361.
[7] S.H. Leala, M.T. Escote, F.M. Pontes, E.R. Leite, M.R. Joya, P.S. Pizani, E. Longo, J.A. Varela, J. Alloys Compd. 475 (2009) 940–945.
[8] K. Bhattacharyya, A.K. Tyagi, J. Alloys Compd. 470 (2009) 580–583.
[9] L. Liu, H. Fan, S. Ke, X. Chen, J. Alloys Compd. 458 (2008) 504–508.
[10] A.S. Bhalla, R. Guo, R. Roy, Mater. Res. Innov. 4 (2000) 3–26.
[11] E. Sawaguchi, H. Maniwa, S. Hoshino, Phys. Rev. 83 (1951) 1078.
[12] S. Roberts, J. Am. Ceram. Soc. 33 (1953) 63–66.
[13] F. Jona, G. Shirane, F. Mazzi, R. Pepinsky, Phys. Rev. 105 (1957) 849–856.
[14] X. Dai, J.F. Li, D. Viehland, Phys. Rev. B 51 (1995) 2651–2655.
[15] E. Sawaguchi, J. Phys. Soc. Jpn. 8 (1951) 615–629.
[16] G. Shirane, Phys. Rev. 86 (1952) 219–227.
[17] B.P. Pokharel, D. Pandey, Phys. Rev. B 65 (2002) 214108.
[18] B.P. Pokharel, D. Pandey, J. Appl. Phys. 86 (1999) 3327–3332.
[19] B. Xu, N.G. Pai, L.E. Cross, Mater. Lett. 34 (1998) 157–160.
[20] Q. Tan, Z. Xu, D. Viehland, J. Mater. Res. 14 (1999) 4251–4258.
[21] H. Chen, C. Yang, J. Zhang, Y. Pei, Z. Zhao, J. Alloys Compd. 486 (2009) 615–620.
[22] D.L. Rubia, M.A. Alonso, R.E. Lopez-Garcia, A.R.D. Frutos, IEEE Trans. Ultrason. Ferroelectr. Freq. Control 56 (2009) 1799–1805.
[23] S. Wirunchit, P. Laoratanakul, N. Vittayakorn, J. Phys. D: Appl. Phys. 41 (2008) 125406.
[24] S. Wirunchit, N. Vittayakorn, J. Appl. Phys. 104 (2008) 024103.
[25] W. Banlue, N. Vittayakorn, Ferroelectrics 382 (2009) 122–126.
[26] W. Banlue, N. Vittayakorn, Appl. Phys. A 93 (2008) 565–569.
[27] N. Vittayakorn, P. Charoonsuk, P. Kasiansin, S. Wirunchit, B. Boonchom, J. Appl. Phys. 106 (2009) 064104.
[28] W. Qu, X. Tan, N. Vittayakorn, S. Wirunchit, M.F. Besser, J. Appl. Phys. 105 (2009) 014106.
[29] H. He, X. Tan, Phys. Rev. B 72 (2005) 024102.
[30] S.A. Halawy, N.E. Fouad, M.A. Mohamed, M.I. Zaki, J. Therm. Anal. Calorim. 82 (2005) 671–675.
[31] R.H. Abu-Eittah, N.G. Zaki, M.M.A. Mohamed, L. Kamel, J. Anal. Appl. Pyrol. 77 (2006) 1–11.